Water entry of double-curvature specimens at high speed: effect of the transverse profile

Emanuele Spinosa[a], **Silvano Grizzi**[a], **Alessandro Iafrati**[a]
a. CNR - Institute of Marine Engineering (Rome, Italy)
Email: emanuele.spinosa@cnr.it

1 Introduction

The present paper continues the experimental studies on the water entry at high horizontal speed of double-curvature specimens, following the presentation at the IWWWFB in 2019 (Iafrati and Grizzi, 2019b). The specimens reproduce the fuselage part that first gets in contact with water. The motivations of the experimental activity are to give more insight on the hydrodynamic phenomena occurring during aircraft ditching, in particular cavitation and ventilation, and to build a useful database needed for the validation of the computational tools to simulate the problem. In Iafrati and Grizzi (2019b) the effect of a different longitudinal curvature was analysed, this works focuses on the effects of a different transverse profile (curvature).

2 Experimental set-up

The experiments are performed in the **High Speed Ditching Facility (HSDF)** of the CNR-INM (Institute of Marine Engineering), described in detail in Iafrati et al. (2015); Iafrati (2016); Iafrati and Grizzi (2019a). In this paper the focus is on the tests at a vertical-to-horizontal velocity ratio of U/V=0.0375 and a pitch angle of 6°.

In order to assess the effect of a different transverse profile on the hydrodynamics, two specimens are analysed, denoted as **S2** and **S3**, having the same profile in the longitudinal plane $x-z$, but a different one in the transverse plane $y-z$. In particular, as shown in Figure in 1, **S2** presents a circular cross-section, whereas **S3** is characterized by an elliptic-circular section, which is much "flatter" in the contact zone. In order to better describe the

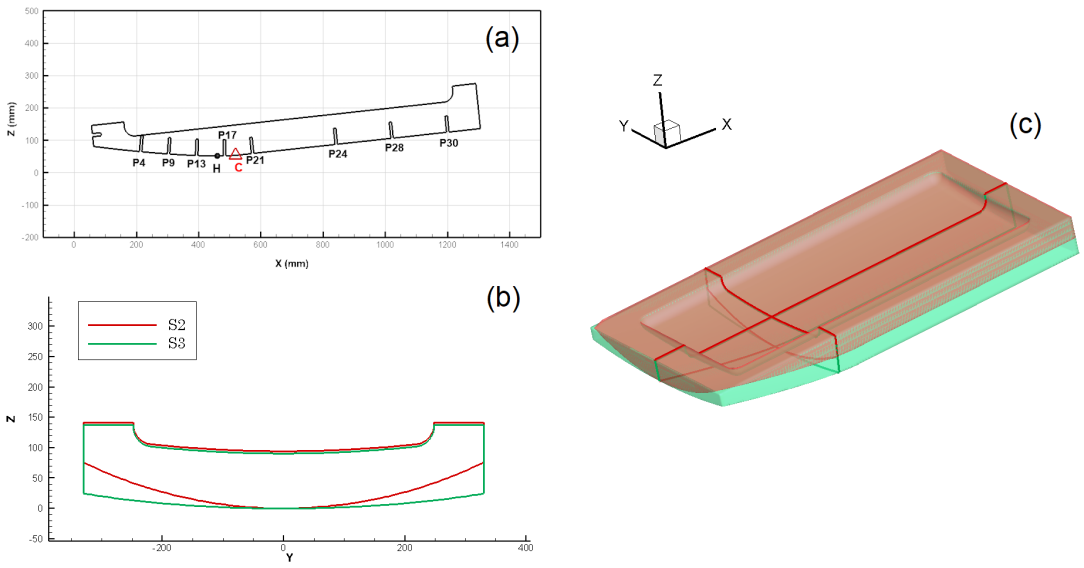

Figure 1: Comparison between the shapes of the two specimens set at a pitch angle of 6°: (a) section on a longitudinal plane (b) section on a transverse plane and (c) 3D view.

hydrodynamics of the water entry, two points are defined, see Figure 1(a): the point **H**, i.e. the lowest point of the specimen at the given attitude and therefore the point that gets in contact with water first, and the point **C**, at which, following the lower profile from the leading to the trailing edge, the profile changes from rectilinear to curved.

A total of 30 pressure probes are installed flush-mounted to the specimen surface. In this paper the focus is on the pressure measurements along the midline (on the plane $x-z$), as shown in Figure 1(a). A total of six load cells are also installed, to measure the normal loads at the front and at the rear and the tangential load. Finally, a high-speed camera is installed underwater to visualize the flow development and to support the experimental data interpretation.

3 Analysis of the experimental data

In order to compare the time histories or forces and pressures at different test conditions, a non-dimensional time is defined as $\tau \doteq (t-t_0)/(t_E-t_0)$, where t_0 is the time of first contact of the specimen with water and t_E is the time at which the spray root reaches the leading edge, which identifies the end of the test. Both t_0 and t_E are estimated by using the pressure data.

The pressures time histories of the probes along the midline are shown in Figure 2 for the tests at a horizontal speed of U=40 m/s. The probes located in front and behind the point **C** are shown in separate graphs. In the figure two underwater video-frames, one shortly after the impact (τ=0.2) and one at about half of the impact phase (τ=0.6), are also shown. These times are marked with vertical lines in the plots with the pressure time histories.

In the **front part** of the wetted area, it is possible to recognize the advancement of the spray, which appears much more intense for the shape **S3**. Such a circumstance is in agreement with the pressure data. In fact, in **S3** the pressure peaks recorded by the probes P21, P24, P28 and P30, see Figure 2(e) and (f), are higher and less noisy. This is because the flatter bottom of the shape **S3** limits the possibility of the fluid to escape, thus leading to higher pressures at the spray root, and behaving similarly to the flat plate impact (Iafrati et al., 2015; Iafrati, 2016).

The pressure probes in the **rear part** (i.e. behind the point **C**), unlike the front probes, do not exhibit any positive peak at the impact time, except for P17, which is located just behind the change of curvature **C**, but ahead point of first contact **H**. On the other hand, for the shape **S3** all the rear probe signals display a series of spikes at the time of impact, possibly corrupted by some undesired noise, indicating the possible presence of a spray propagating backwards. In the underwater video frames at τ=0.2 a cavitation area appears at the rear for both shapes, which is wider in **S3** than in **S2**. In the specimen reference frame, the cavitation area has shape similar to a reversed D. The front edge of the cavitation area remains approximately straight and located at the point of curvature change **C**. On the other side, the curved rear edge expands backwards, as visible in the frames at τ=0.6. When the cavitation area reaches the trailing edge, the ambient pressure forces air to be entrained into the low pressure area, causing a ventilation front quickly propagating towards the leading edge. It is expected that the pressures at the rear are lower in **S3** with respect to **S2**, in agreement with the results shown in Spinosa et al. (2022), in which the planing motion of the same fuselage shapes at a pitch angle of 6° is simulated, albeit at a much lower speed. Looking at the pressure time histories, see Figure 2(g) and (h), when the cavitation front passes over the rear probes P4, P9, P13 and P17, the pressure suddenly drops down to the vapour pressure value. When the ventilation front reaches the probes, the values gradually rise approximately to the zero value, i.e. to the atmospheric pressure values.

The propagation velocity of the rear edge of the cavitation area, denoted as U_{cav}, is estimated using the high-speed video frames, by tracking in time the rearmost point of the cavitation area in the specimen reference frame. The variation of U_{cav} as a function of the horizontal speed, spanning from about U=30 to 45 m/s, is shown in Figure 3. It can be observed that the cavitation velocity varies linearly with the horizontal speed, as confirmed by the very high values of the coefficients of determination R^2 for the least-squared linear fits, displayed in Figure 3. The slopes for **S2** and **S3** are almost equal, suggesting that the trend is strongly related to the longitudinal profile. On the other hand, the offset between the curves could be due to the different transverse profile, but further studies are needed to confirm this assertion.

The measured loads time histories, shown in Figure 4, are consistent with the pressure

(a) Shape **S2** - Frame τ=0.2

(b) Shape **S3** - Frame τ=0.2

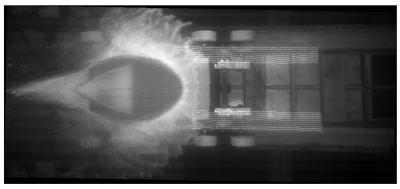

(c) Shape **S2** - Frame τ=0.6

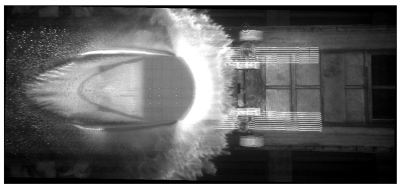

(d) Shape **S3** - Frame τ=0.6

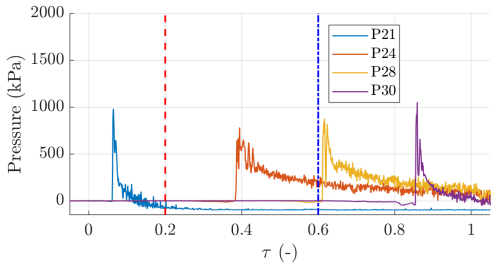

(e) p midline - Front probes - Shape **S2**

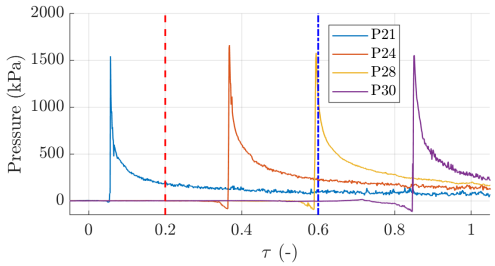

(f) p midline - Front probes - Shape **S3**

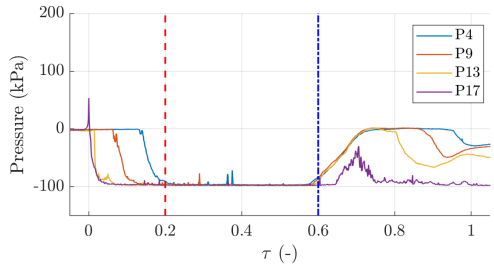

(g) p midline - Rear probes - Shape **S2**

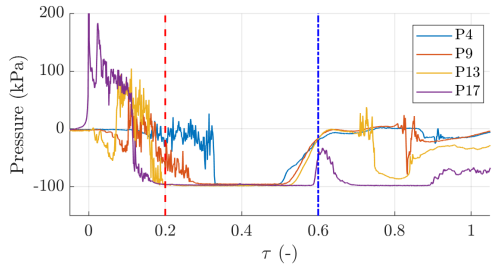

(h) p midline - Rear probes - Shape **S3**

Figure 2: Front and rear midline pressure time histories and under-water frames at τ=0.2 and 0.6 for the two shapes at U=40 m/s, U/V=0.0375 and pitch angle 6°.

signals and with the information derived from the underwater videos. The front cells record an increasing load, related mainly to the positive pressure area developing at the spray root, with higher forces for the shape **S3**. The rear cells, instead, are characterized by an almost constant or slightly negative trend as a result of the negative pressure developing at the rear. Once ventilation occurs, the load measured by the rear cells increases for both shapes, as a result of the pressures rising up to the atmospheric value in the ventilated zone. This occurs earlier in **S3**, than in **S2**, in agreement with what discussed above in terms of pressure.

4 Conclusions

The effect of the different transverse profile in the water entry of double-curvature specimens at high horizontal speed is examined. It is shown that a flatter shape (i.e. **S3**) results in increased pressures at the spray root in front, since the flow has a more limited possibility to escape from the sides. In addition, at the rear a flatter profile causes an earlier initiation of the cavitation phenomena (and so of ventilation) and a higher speed of the rear edge of the cavitation area.

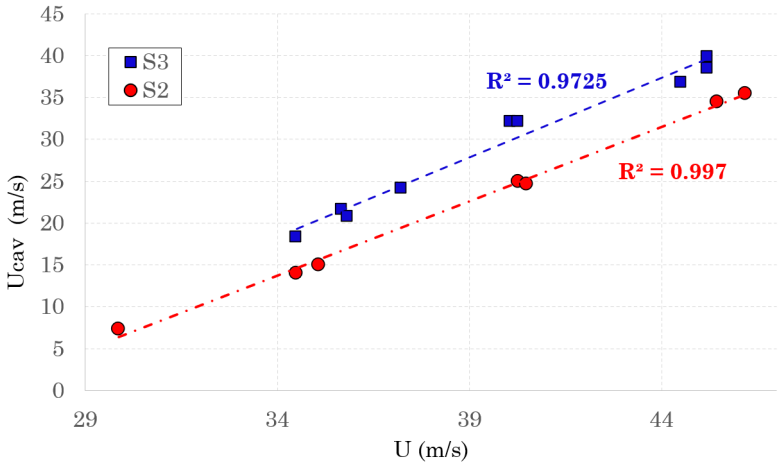

Figure 3: Velocity of the rear edge of the cavitation area U_{cav} as a function of the horizontal speed U for the two shapes.

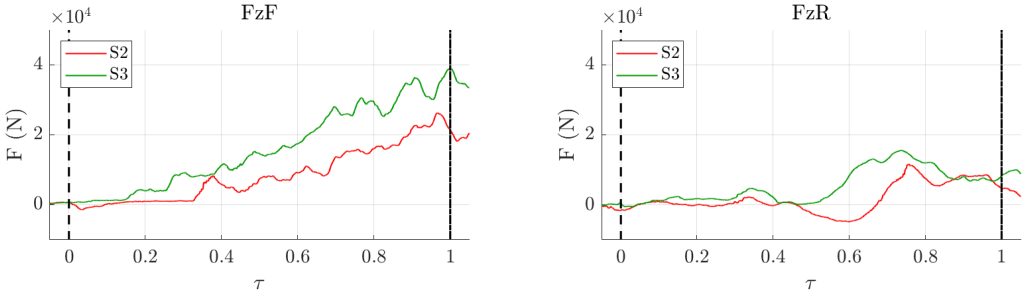

Figure 4: Time histories of the normal forces for the two shapes at U=40 m/s, $U/V = 0.0375$ and pitch angle 6°.

These results is consistent for the whole horizontal speed range, from about U=30 to 45 m/s. More detailed results will be presented at the workshop.

Acknowledgements

This project has been partly funded from the European Union's Horizon 2020 Research and Innovation Programme under Grant Agreement No. 724139 (H2020-SARAH: increased SAfety & Robust certification for ditching of Aircrafts & Helicopters).

References

Iafrati, A. (2016). Experimental investigation of the water entry of a rectangular plate at high horizontal velocity. *Journal of Fluid Mechanics*, 799:637–672.

Iafrati, A. and Grizzi, S. (2019a). Cavitation and ventilation modalities during ditching. *Physics of Fluids*, 31(5):052101.

Iafrati, A. and Grizzi, S. (2019b). Cavitation/ventilation phenomena during the water impact with horizontal velocity of double curvature shaped bodies. International Workshop on Water Waves and Floating Bodies. NewCastle, Australia.

Iafrati, A., Grizzi, S., Siemann, M., and Montañés, L. B. (2015). High-speed ditching of a flat plate: Experimental data and uncertainty assessment. *Journal of Fluids and Structures*, 55:501–525.

Spinosa, E., Broglia, R., and Iafrati, A. (2022). Hydrodynamic analysis of the water landing phase of aircraft fuselages at constant speed and fixed attitude. *Aerospace Science and Technology*, 130:107846.